Published in final edited form as:
Dev Biol. 2014 December 1; 396(1): 8–18. doi:10.1016/j.ydbio.2014.09.031.

Alk3 Mediated Bmp Signaling Controls the Contribution of Epicardially Derived Cells to the Tissues of the Atrioventricular Junction

Marie M. Lockhart[a], **Bastiaan J. D. Boukens**[b], **Aimee L. Phelps**[a], **Christina-Lin M. Brown**[a], **Katelynn A. Toomer**[a], **Tara A. Burns**[a], **Rupak D. Mukherjee**[c], **Russell A. Norris**[a], **Thomas C. Trusk**[a], **Maurice J.B. van den Hoff**[d], and **Andy Wessels**[a,*]

[a]Department of Regenerative Medicine and Cell Biology, Medical University of South Carolina, Charleston, South Carolina, USA [b]Department of Biomedical Engineering, Washington University, St. Louis, Missouri, USA [c]Division of Cardiothoracic Surgery, Department of Surgery and Department of Pediatrics, Medical University of South Carolina, Charleston, South Carolina, USA [d]Heart Failure Research Center, Department of Anatomy, Embryology and Physiology, Academic Medical Center, Amsterdam, The Netherlands

Abstract

Recent studies using mouse models for cell fate tracing of epicardial derived cells (EPDCs) have demonstrated that at the atrioventricular (AV) junction EPDCs contribute to the mesenchyme of the AV sulcus, the annulus fibrosus, and the parietal leaflets of the AV valves. There is little insight, however, into the mechanisms that govern the contribution of EPDCs to these tissues. While it has been demonstrated that bone morphogenetic protein (Bmp) signaling is required for AV cushion formation, its role in regulating EPDC contribution to the AV junction remains unexplored. To determine the role of Bmp signaling in the contribution of EPDCs to the AV junction, the Bmp receptor activin-like kinase 3 (Alk3; or Bmpr1a) was conditionally deleted in the epicardium and EPDCs using the mWt1/IRES/GFP-Cre ($Wt1^{Cre}$) mouse. Embryonic $Wt1^{Cre}$;$Alk3^{fl/fl}$ specimens showed a significantly smaller AV sulcus and a severely underdeveloped annulus fibrosus. Electrophysiological analysis of adult $Wt1^{Cre}$;$Alk3^{fl/fl}$ mice showed, unexpectedly, no ventricular pre-excitation. Cell fate tracing revealed a significant decrease in the number of EPDCs within the parietal leaflets of the AV valves. Postnatal $Wt1^{Cre}$;$Alk3^{fl/fl}$ specimens showed myxomatous changes in the leaflets of the mitral valve. Together these observations indicate that Alk3 mediated Bmp signaling is important in the cascade of events that regulate the contribution of EPDCs to the AV sulcus, annulus fibrosus, and the parietal leaflets of the AV valves. Furthermore, this study shows that EPDCs do not only play a

*Corresponding author: Andy Wessels, Ph.D. Department of Regenerative Medicine and Cell Biology, Medical University of South Carolina, 173 Ashley Avenue, Room BSB-648B, P.O. Box 250508. Charleston, SC 29425. Tel: 843-792-8183, Fax: 843-792-0664, wesselsa@musc.edu.

critical role in early developmental events at the AV junction, but that they also are important in the normal maturation of the AV valves.

Keywords

epicardium; bone morphogenetic protein; myxomatous; valves; development

INTRODUCTION

At approximately embryonic day (ED) 9.0 in the mouse, cells from the proepicardium, a heterogeneous cluster of cells located at the inferior margin of the cardiac sinus venosus, migrate to the dorsal surface of the ventricles and spread over the entire heart to form the epicardium (Viragh and Challice, 1981). The subepicardial space, located between the epicardium and the myocardium, subsequently becomes populated by epicardially-derived cells (EPDCs) resulting from an epicardial epithelial-to-mesenchymal transition (epiEMT).

At the atrioventricular (AV) junction the accumulation of subepicardial mesenchyme gives rise to the AV sulcus (Viragh and Challice, 1981; Wessels et al., 2012; Zhou et al., 2010). Meanwhile, in the AV canal, an endocardial EMT (endoEMT) is responsible for the generation of endocardially derived cells (ENDCs) within the cardiac jelly thus leading to the formation of the major AV cushions (Markwald et al., 1977). In subsequent stages, while the major cushions are fusing, two smaller cushions form on the inside of the lateral AV myocardial junctions and, like the major cushions, these lateral cushions also become populated by ENDCs (de Lange et al., 2004; Wessels et al., 2012). Although the four AV cushions are initially endocardially-derived, the lateral cushions are gradually colonized by EPDCs from the AV sulcus around ED12.5 (Wessels et al., 2012). As a result, the parietal leaflets of the AV valves, which are derived from the lateral AV cushions, are mostly comprised of EPDCs. The cellular content of the septal leaflet of the right AV valve and the aortic leaflet of the mitral valve, which are derived from the major AV cushions, remains predominantly of endocardial origin (Wessels et al., 2012). EPDCs are also involved in the formation of the annulus fibrosus, a fibrous sheet of tissue that functions to separate the atrial and ventricular myocardium at the lower boundary of the AV junction (Wessels et al., 2012). In the maturing heart of mammals and birds, this separation is critical for maintaining sequential electrical activation of atria and ventricles (Jensen et al., 2012). Despite what is known about the contribution of EPDCs to the respective tissues at the developing AV junction, the molecular mechanisms involved have yet to be elucidated.

Previous studies have demonstrated that bone morphogenetic protein (Bmp) signaling is critical to the formation of the AV junction. Bmp2 is expressed at high levels in the myocardium of the AV canal during early embryonic development where it promotes endoEMT and accumulation of cardiac jelly for AV cushion formation (Ma et al., 2005; Rivera-Feliciano and Tabin, 2006). Little to no BMP2 is found in the working myocardium of atria and ventricles (Briggs et al., 2013). In addition to its role in the formation of the AV cushions, Bmp2 also regulates patterning of the AV junctional myocardium through regulation of T-box transcription factors (Ma et al., 2005). It is well established that the Bmp

receptor activin-like kinase 3 (Alk3; or Bmpr1a) is required in the endocardium and myocardium of the AV canal for the induction of endoEMT and, hence, AV cushion formation (Ma et al., 2005; Rivera-Feliciano and Tabin, 2006; Yamada et al., 2000). Later in development, Alk3 is also required for AV valve maturation; conditionally deleting Alk3 from the AV canal myocardium results in AV valve defects as well as malformation of the annulus fibrosus (Gaussin et al., 2005; Gaussin et al., 2002).

Compared to what is known about Bmp signaling in the development of the endocardial AV cushions, little is known about the role of Bmp signaling in AV epicardial development. However, the fact that *in vitro* studies using immortalized murine epicardial cells have demonstrated that Bmp2 signaling regulates epiEMT and invasion through Alk3 (Hill et al., 2012), indicates that this pathway may play a role in the regulation of epicardial related events in the AV junction.

In this paper, we tested the hypothesis that Bmp signaling is required for proper development of epicardially-derived structures at the AV junction. We did this by conditionally deleting the Alk3 receptor from the epicardium and EPDCs using an established epicardial-specific cre transgenic mouse line (Casanova et al., 2012; Wessels et al., 2012). Our data support a mechanism by which Bmp signaling through Alk3 is critical for proper development of the AV sulcus and annulus fibrosus. Furthermore, the conditional deletion of Alk3 significantly restricts the contribution of EPDCs to the developing parietal AV valve leaflets. The reduced number of EPDCs in these leaflets ultimately leads to defects that phenocopy myxomatous valve disease in humans.

MATERIALS AND METHODS

Mice

This study was carried out in accordance with the recommendations in the Guide for the Care and Use of Laboratory Animals of the National Institutes of Health. B6.129(Cg)-Gt(ROSA)26Sor$^{tm4(ACTB-tdTomato,-EGFP)Luo}$/J reporter mice (R26$^{mT/mG}$) were crossed to mWt1/IRES/GFP-Cre (Wt1^{cre}) mice (Wessels et al., 2012) and Alk3$^{flox/flox}$ mice (Mishina et al., 2002). The offspring from these matings were then interbred to obtain Wt1^{cre};Alk3$^{+/+}$;R26^{mG} (control), Wt1^{cre};Alk3$^{fl/+}$;R26^{mG}, and Wt1^{cre};Alk3$^{fl/fl}$;R26^{mG} offspring. Embryos were collected from timed pregnant dams and staged as described before (Wessels et al., 2012).

Histology

Embryos were fixed in 4% paraformaldehyde (PFA) for 4 hours before being dehydrated in graded alcohols, cleared in toluene, and embedded in paraffin. 5μm tissue sections were used for Hematoxylin and Eosin staining, immunohistochemistry, and *in situ* hybridization. For immunohistochemistry, tissue was deparaffinized in xylenes and rehydrated in graded alcohols. Antigen retrieval was performed by boiling slides in antigen unmasking solution in a pressure cooker for five minutes. Prior to immunolabeling, tissues were pretreated with 1% BSA in PBS for 1 hour before to prevent non-specific antibody binding. Antibodies were diluted in PBS at the following concentrations: Alk3/BmprIa(E-16) 1:50 (goat, Sana Cruz sc

-5676); Cleaved Caspase-3(Asp175) (1:200; rabbit, Cell Signaling 9664); collagen I (1:200; rabbit, MD Bioproducts 203002); Hyaluronic Acid Binding Protein (HABP) (4μg/mL; biotinylated, Seikagaku Biobusiness 400763-1A); ki67 (1:100; rat, Dako M7249); phosphorylated-Smad-1/5/8 (1:100; rabbit, Millipore AB3848); anti-eGFP (1:500; chicken, Abcam ab13970); Myosin Heavy Chain/MF20 (1:50; mouse, DSHB), Myosin Heavy Chain β (1:500; mouse, Millipore MAB1628), and Myosin Light Chain 2a (1:4000; rabbit, (Kubalak et al., 1994)). Nuclei were visualized using DAPI (Slowfade Gold Antifade Reagent with DAPI, Invitrogen S36938). Fluorescence was visualized using a Zeiss AxioImager II microscope. *In situ* hybridization was performed with digoxigenin (DIG)-labeled probes specific to Bmp2 and Bmp4 as previously described(Kruithof et al., 2006).

AV Sulcus Area

AV sulcus area at ED13 was quantified in Image J software by outlining the sub-epicardial mesenchyme at the AV junction in a 40X field of view. To maintain consistent measurements between specimens, the AV sulcus was placed in the same orientation for each 40X image with the upper boundary of the AV groove positioned at the top of the field of view. Each measurement was performed on four sections spaced 25 μm apart for five control and five $Wt1^{cre};Alk3^{fl/fl};R26^{mG}$ specimens.

Cell proliferation

To quantify proliferation in the ED13 AV sulcus, the number of ki67 positive cells and DAPI positive nuclei were counted in a 40X field of view of four sections, spaced 25 μm apart, for five control and five $Wt1^{cre};Alk3^{fl/fl};R26^{mG}$ specimens. To assess the level of proliferation in P1 neonatal left parietal and aortic leaflets (LPL and AL respectively), the total number of DAPI positive nuclei and the amount of ki67 positive cells was totaled for both the eGFP and non-eGFP labeled cell populations. This analysis was performed on ten LPL-containing sections and five AL-containing sections spaced 25 μm apart, in three controls and three $Wt1^{cre};Alk3^{fl/fl};R26^{mG}$ specimens. Percent proliferation for the total number of valve cells was calculated by dividing the number of ki67-positive cells by the number of DAPI-positive nuclei within each LPL. Percent proliferation for EPDCs was calculated by dividing the number of ki67+/eGFP+ cells by the number of GFP+/DAPI+ cells within the leaflet. Percent proliferation for non-EPDCs was calculated by dividing the number of ki67+/eGFP- cells by the number of eGFP-/DAPI+ cells within the leaflet.

Apoptosis

To quantify apoptosis in the ED13 AV sulcus, the number of Cleaved-Caspase 3 positive cells and DAPI positive nuclei were counted in a 40X field of view on two sections spaced 25 μm apart in four control and three $Wt1^{cre};Alk3^{fl/fl};R26^{mG}$ specimens.

AMIRA 3D reconstruction and volume quantification

To reconstruct eGFP expression within each leaflet of ED15, ED17, and P1 neonatal control, $Wt1^{cre};Alk3^{fl/+};R26^{mG}$, and $Wt1^{cre};Alk3^{fl/fl};R26^{mG}$ specimens, serial 5μm sections spanning the entirety of the AV junction were immunolabeled with antibodies to MF20 and eGFP. Nuclei were stained with DAPI. Image files were uploaded to AMIRA imaging

software and 3D reconstructions of each leaflet were made by tracing the outline of each leaflet using MF20 to mark the myocardium and DAPI to mark all nuclei. To reconstruct eGFP expression within the leaflet, the thresholding tool feature was used to select all eGFP positive cells within the area of the traced leaflet. The volume occupied by eGFP positive voxels within the leaflet and the volume occupied by the entire leaflet were calculated using the Material Statistics tool in AMIRA. By dividing the volume of the eGFP labeled area by the volume of the leaflet labeled area, the percentage of eGFP labeled cells within the leaflet was calculated. A minimum of three specimens was use for reconstructions of eGFP expression at each stage, with the exception of the ED17 control, where only two specimens were used. To calculate leaflet volume in non-eGFP labeled neonatal specimens, 3D reconstructions were created using serial sections from a minimum of five Hematoxylin and Eosin stained hearts from control and $Wt1^{cre}$;$Alk3^{fl/fl}$ specimens.

ECG analysis

To record electrocardiograms (ECG), male $Wt1^{cre}$;$Alk3^{fl/fl}$ mice and control littermates ages 4-8 weeks were anesthetized with isoflurane and maintained in 1.5% isoflurane/5% oxygen while supine on a heated mat. Three subdermal electrodes were inserted into the two forelimbs and the left hindlimb. ECGs were amplified and captured at 2.5 kHz (PONEMAH, Data Sciences International) in Leads I, II, and III configurations. Data analysis and interval calculations were made in Excel using ten example waveforms for each mouse. The PR interval was defined as the time from the start of the P wave to the first deflection of the QRS complex. The iso-electric line was defined as the line connecting the end of the T wave and the start of the P wave of the next beat. The start of the QRS complex was defined as the earliest moment of deviation from baseline. The end of the QRS complex determined in lead III and was defined as the moment when the S wave returned to the isoelectric line (Boukens et al., 2013). We determined the end of the T wave by the tangent method (Lepeschkin and Surawicz, 1952). QTc was calculated according to Mitchell et al (Mitchell et al., 1998).

Mitral Valve Cell Counts

To quantify the number of cells in the LPL and AL of the mitral valve, cells were counted in four $50\mu m^2$ areas within the LPL or AL on four equivalently spaced sections from 3-4, one month old control and $Wt1^{cre}$;$ALk3^{fl/fl}$ hearts. The cell count data is expressed as the average number of cells per $50\mu m^2$.

Statistics

An unpaired, two-tailed Student’s T-test was used to calculate significance in Excel at $p<0.05$. Error is represented as standard error of the mean.

RESULTS

Bmp signaling in the AV junction

To determine whether Alk3 is expressed in the epicardium and EPDCs in the AV junction, immunolabeling was performed on ED13 wildtype hearts. This showed strong expression of Alk3 in the AV sulcus and weaker labeling in the myocardium (Figure 1A). To test whether canonical Bmp signaling is active in the EPDCs at the AV junction, immunolabeling for

phospho-Smad-1/5/8 was performed. Within the AV junction of ED13 wildtype hearts, strong phospho-Smad-1/5/8 labeling was found in the epicardium/EPDCs of the AV sulcus and endocardium, whereas weaker labeling was observed in the AV myocytes (arrows Figure 1B).

Alk3 functions as a receptor for Bmp2, Bmp4, Bmp6, and Bmp7(van Wijk et al., 2007). Mutations in Bmp2 or Bmp4 result in defects in the AV junction while mutations in Bmp6 or Bmp7 do not cause cardiac malformations (van Wijk et al., 2007). Given that Bmp2 and Bmp4 are critical for AV junctional development (Jiao et al., 2003; Ma et al., 2005), section *in situ* hybridization was performed for Bmp2 and Bmp4 at ED13.5 in order to ascertain which of these Alk3 ligands might be involved in regulating the contribution of EPDCs to the development of the AV sulcus and the AV valves. In agreement with previously published data, expression of Bmp2 mRNA (Figure 1C) was found in the AV junctional myocardium. Expression of Bmp4 mRNA was observed in the epicardium as well as the EPDCs in the AV sulcus (Figure 1D).

$Wt1^{cre}$ mediated deletion of Alk3 leads to postnatal lethality

In order to determine the importance of Bmp signaling through Alk3 for epicardial development and to trace the epicardial cell lineage in this experimental setting, Alk3 was conditionally deleted by crossing $Wt1^{cre}$ mice to $Alk3^{fl/fl}$ and $R26R^{mT/mG}$ reporter mice to generate $Wt1^{cre}$;$Alk3^{+/+}$;$R26^{mG}$ (control) $Wt1^{cre}$;$Alk3^{fl/+}$;$R26^{mG}$, and $Wt1^{cre}$;$Alk3^{fl/fl}$;$R26^{mG}$ animals. Using this approach 92 litters were collected spanning time points from ED9.5 to adult animals. $Wt1^{cre}$;$Alk3^{fl/fl}$;$R26^{mG}$ mice were born at the expected Mendelian ratios. Although no size differences were detected at birth, $Wt1^{cre}$;$Alk3^{fl/fl}$;$R26^{mG}$ mice exhibited failure to thrive and by 4 weeks of age only achieved about half the body weight of control animals (Figure 2). Approximately 48% of $Wt1^{cre}$;$Alk3^{fl/fl}$;$R26^{mG}$ mice died unexpectedly or required euthanization due to poor physical condition between weaning and 6 weeks of age. Detailed histopathological examination of a $Wt1^{cre}$;$Alk3^{fl/fl}$;$R26^{mG}$ mouse identified numerous cysts and hyperplastic areas within the colonic epithelium as well as a shortened small intestine (data not shown), suggesting that the premature death of $Wt1^{cre}$;$Alk3^{fl/fl}$;$R26^{mG}$ mice could be associated with these intestinal abnormalities.

Epicardial-specific deletion of Alk3 does not affect the development of the proepicardium, the formation of the epicardium, or the migration of EPDCs into the ventricular walls

To determine whether the conditional deletion of Alk3 using the $Wt1^{cre}$ mice interferes with the initial development of the proepicardium, $Wt1^{cre}$;$Alk3^{fl/fl}$;$R26^{mG}$ and littermate control specimens were examined at ED9.5. The histological analysis showed no differences in the formation of the proepicardium between control and $Wt1^{cre}$;$Alk3^{fl/fl}$;$R26^{mG}$ specimens (Figure 3A,B). We also did not observe any abnormalities in the formation of the epicardium over the surface of the heart. Moreover, the migration of EPDCs into the ventricular walls of $Wt1^{cre}$;$Alk3^{fl/fl}$;$R26^{mG}$ specimens was also found to be unaffected as eGFP labeled EPDCs were found throughout the compact myocardium at ED17 in a pattern indistinguishable from control hearts. Furthermore, EPDCs also appeared to contribute normally to the coronary vasculature (Figure 3C,D).

Epicardial-specific deletion of Alk3 results in abnormalities in the AV sulcus

The AV sulcus is an epicardially-derived tissue formed by epiEMT (Viragh and Challice, 1981; Wessels et al., 2012; Zhou et al., 2010). To test whether Alk3 had been successfully deleted from the AV-EPDCs, immunolabeling was performed for Alk3 in control and $Wt1^{cre}$;$Alk3^{fl/fl}$;$R26^{mG}$ hearts. At ED13, $Wt1^{cre}$;$Alk3^{fl/fl}$;$R26^{mG}$ specimens showed reduced Alk3 expression in the EPDCs of the AV sulcus (Figure 4A, D) and the spatiotemporal pattern of EPDC distribution within the AV junction was altered (Figure 4B, E). In control specimens at this age numerous EPDCs were found migrating into the AV canal myocardium (Figure 4C, arrowheads). In contrast, in the AV myocardium of ED13 $Wt1^{cre}$;$Alk3^{fl/fl}$;$R26^{mG}$ hearts just a few EPDCs were observed (Figure 4F, arrowheads).

At ED13, the AV sulci of $Wt1^{cre}$;$Alk3^{fl/fl}$;$R26^{mG}$ hearts are hypoplastic (Figure 5A-F). Quantification of the AV sulcus area in ED13 control and $Wt1^{cre}$;$Alk3^{fl/fl}$;$R26^{mG}$ hearts, revealed that it was reduced by approximately 28% on left and right sides of the AV junction (Figure 5G). Although there were no significant differences in the number of epicardial cells overlying the AV sulci (data not shown), significantly fewer EPDCs were found within the AV sulci of $Wt1^{cre}$;$Alk3^{fl/fl}$;$R26^{mG}$ specimens at ED13 (Figure 5H), resulting in a 37% decrease in the ratio of EPDCs to epicardial cells in the left AV sulcus and a 71% decrease in the ratio of EPDCs to epicardial cells in the right AV sulcus (Figure 5I).

Bmp signaling through Alk3 has been demonstrated to be involved in regulating proliferation during cardiac development (Briggs et al., 2013). To determine whether the reduction in the number of AV-EPDCs in conditional knockout embryos results from reduced proliferation of AV-EPDCs, ki67 immunolabeling was performed on ED13 control and $Wt1^{cre}$;$Alk3^{fl/fl}$;$R26^{mT/mG}$ hearts. Quantification of the number of ki67 positive cells and the total number of EPDCs in the AV sulcus showed that although there was a significant reduction in the total number of EPDCs in the AV sulcus, the percentage of proliferating EPDCs within the AV sulcus was unchanged in control and $Wt1^{cre}$;$Alk3^{fl/fl}$;$R26^{mG}$ specimens (Figure 5J). Additionally, no change in the percentage of proliferating epicardial cells overlying the AV junction area was observed (Figure 5K). To determine whether the reduction in AV-EPDCs in $Wt1^{cre}$;$Alk3^{fl/fl}$;$R26^{mG}$ specimens is due to increased apoptosis of AV-EPDCs, ED13 $Wt1^{cre}$;$Alk3^{fl/fl}$;$R26^{mG}$ and control specimens were immunolabeled for cleaved Caspase 3. No significant difference in the number of cleaved Caspase-3 positive cells was observed in the AV sulci (Figure 5L).

Alk3 is required for the formation of the annulus fibrosus

Because the annulus fibrosus is an epicardially-derived tissue (Viragh and Challice, 1981; Wessels et al., 2012; Zhou et al., 2010) and is in continuity with the AV sulcus, we hypothesized that its development would also be compromised in $Wt1^{cre}$;$Alk3^{fl/fl}$ hearts. Immunolabeling for periostin and collagen-I was performed on ED17 control and $Wt1^{cre}$;$Alk3^{fl/fl}$ hearts to visualize the annulus fibrosus (Zhou et al., 2010). While in control hearts a well-formed annulus fibrosus was present, in $Wt1^{cre}$;$Alk3^{fl/fl}$ hearts this fibrous tissue boundary was missing (Figure 6A-F). This phenotypical difference was more pronounced in the left than in the right AV junction.

To delineate atrial and ventricular myocardium at the AV junction, ED17 specimens were immunolabeled using antibodies for the atrial marker Myosin Light Chain 2a (MLC2a) and the ventricular marker Myosin Heavy Chain-β (MHCβ). In control ED17 specimens, the annulus fibrosus creates a distinct separation of atrial and ventricular myocytes, whereas in $Wt1^{cre};Alk3^{fl/fl}$ hearts this distinct boundary is lost. Interestingly, even though in these $Wt1^{cre};Alk3^{fl/fl}$ hearts the annulus fibrosus was absent, the distinct expression pattern of MLC2a and MHCβ remained unaltered (Figure 6G,H).

$Wt1^{cre};Alk3^{fl/fl};R26^{mG}$ mice do not exhibit ventricular pre-excitation

As described above, in $Wt1^{cre};Alk3^{fl/fl}$ and $Wt1^{cre};Alk3^{fl/fl};R26^{mG}$ embryonic hearts we observe disruption of the annulus fibrosus, a tissue critical for separating atrial and ventricular myocardium. Previous work in chicken has demonstrated that in pro-epicardial inhibited embryos, annulus fibrosus formation is disrupted resulting in a shortened P-R interval and ventricular pre-excitation (Kolditz et al., 2008). Therefore, we hypothesized that $Wt1^{cre};Alk3^{fl/fl}$ mice would exhibit a similar conduction abnormality. To investigate this, electrocardiogram (ECG) analysis was performed. This showed, against expectation, no changes in the duration of the PR, QRS, or RR intervals in $Wt1^{cre};Alk3^{fl/fl}$ mice when compared to control littermates (Table 1). Additionally, the presence of a delta wave, which would have been indicative of ventricular pre-excitation, was not observed in any of the $Wt1^{cre};Alk3^{fl/fl}$ mice.

Alk3 is required for EPDC contribution to the leaflets of the AV valves

Using the $Wt1^{cre};R26^{mG}$ mouse, we have previously demonstrated that EPDCs preferentially contribute to the parietal leaflets of the AV valves (Wessels et al., 2012). Given the abnormal development of the AV sulcus and annulus fibrosus in $Wt1^{cre};Alk3^{fl/fl}$ and $Wt1^{cre};Alk3^{fl/fl};R26^{mG}$ specimens, we hypothesized that the contribution of EPDCs to the parietal leaflets could also be compromised. In order to assess the contribution of EPDCs to the AV valve leaflets in $Wt1^{cre};Alk3^{fl/fl};R26^{mG}$ hearts, eGFP immunolabeling was performed on ED17 control (Figure 7A,B) and $Wt1^{cre};Alk3^{fl/fl};R26^{mG}$ (Figure 7C,D) specimens. This staining revealed a reduction in the numbers of EPDCs within the parietal leaflets of the AV valves of $Wt1^{cre};Alk3^{fl/fl};R26^{mG}$ hearts (Figure 7A-D).

Spatiotemporal analysis of EPDC contribution to the AV valve leaflets

In order to evaluate the spatiotemporal contribution of EPDCs to the parietal leaflets of the AV valves and to quantify the percentage of EPDCs within these leaflets throughout development, serial sections spanning the entire AV junction of control, $Wt1^{cre};Alk3^{fl/+};R26^{mG}$, and $Wt1^{cre};Alk3^{fl/fl};R26^{mG}$ specimens were immunolabeled for eGFP at ED15, ED17, and postnatal day 1 (P1). Using AMIRA software, the eGFP expression within the left and right parietal leaflets was reconstructed (Figure 8A-T). These reconstructions showed that in ED15 control specimens, EPDCs were predominantly located on the posterior edge of the right parietal leaflet (RPL), while in the left parietal leaflet (LPL) they were localized on the anterior side (Figure 8A, B). In the RPL and LPL at ED17, EPDCs were distributed across the anterior-posterior axis of the leaflet and from the annulus fibrosus to the distal tip of the leaflet where it connects to the papillary muscle (Figure 8C, D). In the LPL of neonatal control hearts, EPDCs were evenly distributed throughout the

anterior-posterior and superior-inferior axes of the leaflet (Figure 8E, M-O). In ED15, ED17, and neonatal $Wt1^{cre}$;$Alk3^{fl/fl}$;$R26^{mG}$ hearts there was a marked reduction in the amount of EPDCs in the LPL and RPL when compared to controls (Figure 8G-L, P-R).

Quantification of EPDC contribution to the leaflets of the AV valves

In order to estimate the percentage of EPDCs within the AV valves in control, $Wt1^{cre}$;$Alk3^{fl/+}$;$R26^{mG}$, and $Wt1^{cre}$;$Alk3^{fl/fl}$;$R26^{mG}$ ED15, ED17, and neonatal specimens, the volume of eGFP immunolabeled pixels and the volume of each leaflet were determined using AMIRA software. In all stages examined, the percentage of the leaflet volume occupied by eGFP-positive cells (EPDCs) was significantly reduced in the LPL and RPL of $Wt1^{cre}$;$Alk3^{fl/fl}$;$R26^{mG}$ specimens (Figure 8U,V). In $Wt1^{cre}$;$Alk3^{fl/+}$;$R26^{mG}$ hearts, the LPL also had a significant reduction in the percentage of EPDCs within the leaflet at ED15 (Figure 8U). In the RPL, however, a significant difference in the percent eGFP was not observed (Figure 8V).

Reduced EPDC contribution results in enlarged neonatal mitral valve leaflets

To determine the effect that reduced numbers of EPDCs in the parietal leaflets have on size and morphology of AV valves, histological (Figure 9A,B) and volumetric analysis (Figure 9C-E) was performed on P1 control and $Wt1^{cre}$;$Alk3^{fl/fl}$;$R26^{mG}$ hearts. In $Wt1^{cre}$;$Alk3^{fl/fl}$;$R26^{mG}$ specimens, the LPL of the mitral valve was significantly increased by 16% ($p=0.04$) over controls. The volume of the aortic leaflet trended towards a significant increase ($p=0.09$) while the volumes of the septal leaflet and RPL of the right AV valve were not significantly different when compared to the control leaflets (Figure 9E).

Loss of EPDCs in the AV junction results in myxomatous changes in the mitral valve

Given that the LPL of the mitral valve is significantly enlarged in the neonatal heart of $Wt1^{cre}$;$Alk3^{fl/fl}$;$R26^{mG}$ specimens, we next examined the mitral valve morphology of $Wt1^{cre}$;$Alk3^{fl/fl}$;$R26^{mG}$ and control specimens at 4-20 weeks of age. Qualitative analysis of $Wt1^{cre}$;$Alk3^{fl/fl}$;$R26^{mG}$ hearts suggested that 9 out of the 17 specimens examined (53%) had increased leaflet size (leaflet elongation, and leaflet thickening) of both the aortic leaflet and LPL compared to littermate controls (Figure 10). In 2 specimens we observed increased LPL size only, and 1 specimen showed isolated increase in the size of the aortic leaflet. The remaining 5 specimens did not exhibit any significant abnormalities in leaflet morphology based on histological analysis.

In the human condition mitral valve prolapse (MVP), myxomatous degeneration of the leaflets is often observed and is thought to be a contributing factor in the pathogenesis of the disease (Hayek et al., 2005). Histological observations in MVP include increased expression of proteoglycans and glycosaminoglycans (GAGs) within the leaflet (Gupta et al., 2009). To determine if the expression of GAGs and proteoglycans were expanded in the postnatal $Wt1^{cre}$;$Alk3^{fl/fl}$;$R26^{mG}$ heart, immunolabeling for the proteoglycan versican-β and the GAG hyaluronan was performed on a $Wt1^{cre}$;$Alk3^{fl/fl}$;$R26^{mG}$ 4 week old specimen with an enlarged LPL as well as on a littermate control. In the control heart, versican-β and hyaluronan expression was found in the distal tip of the properly formed LPL and aortic leaflet (Figure 10A-C), while the enlarged distal portion of the LPL of the

$Wt1^{cre}$;$Alk3^{fl/fl}$;$R26^{mG}$ specimen, contained abnormally large amounts of hyaluronan and versican-β indicating a myxomatous phenotype (Figure 10D-F).

Reduced EPDC contribution to the LPL of the neonatal mitral valve leads to an imbalance in proliferative activity of EPDCs and non-EPDCs

To determine whether an increase in proliferation could be the underlying mechanism leading to the increased leaflet size, proliferation was evaluated by ki67 staining in the LPL of neonatal control and $Wt1^{cre}$;$Alk3^{fl/fl}$;$R26^{mG}$ hearts. In the $Wt1^{cre}$;$Alk3^{fl/fl}$;$R26^{mG}$ specimens, the average number of cells in each leaflet was not significantly different from controls, nor was the overall percentage of proliferating cells significantly different (Table 2). Co-labeling with eGFP antibody was conducted to distinguish EPDCs from non-EPDCs. Comparing the proliferating cohorts of EPDCs and non-EPDCs revealed that EPDCs in the LPL of the $Wt1^{cre}$;$Alk3^{fl/fl}$;$R26^{mG}$ heart were more proliferative than the EPDCs in the LPL of the control heart. The level of proliferation of non-EPDCs was not statistically significant. Analysis of proliferation in the AL in control and $Wt1^{cre}$;$Alk3^{fl/fl}$;$R26^{mG}$ specimens also showed no significant differences in cell number or proliferation (data not shown).

Given that EPDCs in the P1 LPL of $Wt1^{cre}$;$Alk3^{fl/fl}$;$R26^{mG}$ mice are slightly more proliferative than those of controls and that leaflet enlargement is observed in the LPL and AL of adult animals, cell numbers were assessed in 1 month old control and $Wt1^{cre}$;$Alk3^{fl/fl}$;$R26^{mG}$ mitral valves. In the LPL, the average number of cells per $50\mu m^2$ is 13.6 ± 2.4 in controls and 18.4 ± 7.3 in $Wt1^{cre}$;$Alk3^{fl/fl}$;$R26^{mG}$ mice, however this difference is not significant ($p=0.51$). In the AL, the average number of cells per $50\mu m^2$ is 16.2 ± 2.9 in controls and 15.6 ± 2.8 in $Wt1^{cre}$;$Alk3^{fl/fl}$;$R26^{mG}$ mice and this difference is also not statistically significant ($p=0.87$) (Figure 11).

DISCUSSION

While the requirement for Bmp signaling in the formation of the AV junction is well established (Gaussin et al., 2002; Ma et al., 2005; Rivera-Feliciano and Tabin, 2006; Song et al., 2007), the role of EPDCs in the formation of AV junctional tissues has only recently become appreciated (Wessels et al., 2012; Zhou et al., 2010). Here we present data showing that conditional deletion of the Bmp receptor Alk3 in the epicardial lineage using the $Wt1^{cre}$ mouse results in hypoplasia of the AV sulcus, malformation of the annulus fibrosus, and decreased contribution of EPDCs to the parietal leaflets of the AV valves. Despite the significant reduction in the number of EPDCs that migrate into the leaflets, the AV valves develop relatively normally throughout fetal life. In the post-natal heart the reduction of EPDCs within the parietal leaflets of both the left and right AV valve only leads to a significant abnormality of the left AV valve. The right AV valve remains by and large unaffected and to date it is unclear why there are significant differences between the two sides of the heart. The reduced numbers of EPDCs in the LPL results in the enlargement of this leaflet, alterations in cell proliferation, and a myxomatous valve phenotype. Based on the observed abnormal development of the annulus fibrosus, we predicted ventricular pre-excitation would occur. However, in our electrophysiological studies, no abnormalities in AV conduction were found.

$Wt1^{cre}$;$Alk3^{fl/fl}$;$R26^{mG}$ mice do exhibit failure to thrive and premature death. Examination of $Wt1^{cre}$;$Alk3^{fl/fl}$;$R26^{mG}$ mice revealed abnormalities in the gastrointestinal tract, leading us to hypothesize that hyperplasia and dysplasia of the colon and intestines may be the cause of death. This result is not surprising given that the $Wt1^{cre}$ mouse used for this study has cre recombinase activity in the serosal mesothelium and vascular smooth muscle cells of the gut (Wilm et al., 2005). Additionally, Bmp signaling has been demonstrated to be required for normal gastrointestinal tract development, including in the smooth muscle cells of the gut (Barbara et al., 2005; Torihashi et al., 2009).

Bmp signaling and formation of the AV sulcus

Deleting Alk3 in the epicardium and EPDCs inhibits the proper formation of the AV sulcus. The AV sulcus is an epicardially-derived structure that forms early in cardiac development by an accumulation of sub-epicardial mesenchyme at the AV junction. Although cells of the AV sulcus originate from epiEMT (Viragh and Challice, 1981), the relative contribution of epiEMT and the proliferation of EPDCs to the maintenance of the sulcus is unknown. In $Wt1^{cre}$;$Alk3^{fl/fl}$;$R26^{mG}$ specimens at ED13 the AV sulcus is reduced in size when compared to controls and contains fewer EPDCs. While the number of epicardial cells overlying the AV sulcus remains unaltered, assessment of proliferation and apoptosis within the AV sulcus and in the overlying AV junctional epicardium reveals that neither of these processes is responsible for the observed reduction in the number of EPDCs. A similar observation has also been reported for the Tbx2 knockout mouse and the $Myh6^{cre}$;$Tbx2^{fl/fl}$ mice (Aanhaanen et al., 2011). In these mouse models, the AV sulcus also fails to develop normally, yet proliferation and apoptosis are unaffected.

These results suggest that epiEMT may be a critical process for maintaining the cell population within the AV sulcus and that Bmp signaling, through Alk3, is required. In *in vitro* studies with immortalized mouse epicardial cells it was demonstrated that the canonical Alk3 signaling pathway is important in mediating epicardial EMT and invasion by Bmp2 and TgfβIII (Hill et al., 2012). It is therefore becoming increasingly clear that multiple receptors in the TGFβ and Bmp families are important for mediating epicardial EMT through both canonical and non-canonical pathways (von Gise and Pu, 2012).

Conduction Abnormalities

In chicken embryos with a proepicardium-block, the annulus fibrosus fails to properly form, resulting in the persistence of AV myocardial accessory pathways and ventricular pre-excitation (Kolditz et al., 2008). In mice, Mlc2v-cre activation of Notch, conditional deletion of Alk3 from the AV canal myocardium using cGATA6-cre (Gaussin et al., 2005), and conditional deletion of Tbx2 using Myh6-cre all result in ventricular pre-excitation and shortening of the PR interval. Despite subtle differences between the histological and molecular characteristics of these mouse models, collectively these studies demonstrate that both the disruption of annulus fibrosus formation and/or faulty patterning of the AV myocardium can give rise to the formation of accessory pathways and result in ventricular pre-excitation as seen in Wolff-Parkinson-White (WPW) syndrome. Combined, our studies and the ones described above demonstrate that both EPDCs as well as the myocardium of the AV canal play an important role in the formation of the annulus fibrosus.

$Wt1^{cre}$;$Alk3^{fl/fl}$;$R26^{mG}$ mice exhibit malformation of the annulus fibrosus during embryonic development and incomplete separation of AV myocardium postnatally. However, instead of ventricular pre-excitation, no conduction abnormalities are observed in these animals. Bmp signaling is important for the patterning of the AV myocardium, as Bmps regulate the expression of multiple T-box family members, including Tbx2 and Tbx3 (Yamada et al., 2000). Bmp activation of Tbx2 within the AV canal during embryonic development results in the AV canal retaining a primary myocardium phenotype of slow conductance (Aanhaanen et al., 2011). This slow conducting property of the AV myocardium allows for a delay of the cardiac impulse at the AV junction necessary for sequential activation of atrial and ventricular myocardium in the embryonic heart of birds and mammals before the establishment of a mature conduction system and annulus fibrosus. The patterning of the AV myocardium by Tbx2 and Bmp2 is also sufficient to generate AV delay in the adult heart of ectothermic vertebrates such as fish, frogs, and lizards, despite the absence of an annulus fibrosus (Jensen et al., 2012). Given that Alk3, Bmp2, and Tbx3 expression within the AV canal myocardium are not targeted by the epicardial-specific inactivation of Alk3 performed in this study, we hypothesize that the absence of ventricular pre-excitation observed in $Wt1^{cre}$;$Alk3^{fl/fl}$;$R26^{mG}$ mice is possibly due to the retention of normal patterning of the AV canal myocardium in these animals.

Myxomatous mitral valve phenotype

MVP is the most common cause of non-ischemic mitral regurgitation with an estimated prevalence of 2-3% (Hayek et al., 2005). In both syndromic and the more common, non-syndromic forms of MVP, myxomatous changes to the mitral valve leaflets are common and are characterized by increased accumulations of GAGs and proteoglycans in the spongiosa layer of the leaflet (Dietz et al., 1991; Gupta et al., 2009; Jaffe et al., 1981). Alongside these changes, increased expression of matrix metalloproteases (MMPs) (Rabkin et al., 2001) and disorganization of collagen and elastin fibers are also observed (Tamura et al., 1995). Consistent with these previous findings, the leaflets of the left AV valve in post-natal and adult $Wt1^{cre}$;$Alk3^{fl/fl}$;$R26^{mG}$ specimens were morphologically abnormal and myxomatous, containing larger than normal amounts of the proteoglycan versican-β and the GAG hyaluronan. In the fibrillin-1 Marfan syndrome/MVP mouse model, myxomatous mitral valve morphology similar to what is seen in post-natal $Wt1^{cre}$;$Alk3^{fl/fl}$;$R26^{mG}$ specimens is also observed (Ng et al., 2004). Although alterations in proliferation of EPDCs are observed in the neonatal $Wt1^{cre}$;$Alk3^{fl/fl}$;$R26^{mG}$ LPL, these changes do not affect the overall percentage of proliferating cells, nor does this result in a significant increase in cell number in the adult leaflets. These data indicate that proliferation may not be a driving factor in the myxomatous changes observed in $Wt1^{cre}$;$Alk3^{fl/fl}$;$R26^{mG}$ specimens, but instead valve enlargement may be a consequence of excess proteoglycan and hyaluronan content.

The influx of EPDCs into the AV valves coincides with the timing of significant changes in the ECM organization and the onset of cellular condensation (Kruithof et al., 2007), indicating that EPDCs may serve to influence valve maturation. However, the mechanisms by which EPDCs and ENDCs interact within the valve to direct normal development remain unclear. In the $Wt1^{cre}$;$Alk3^{fl/fl}$;$R26^{mG}$ mouse model, the relative contributions of EPDCs and ENDCs within the parietal leaflets are significantly altered and are associated with valve

abnormalities. The excess proteoglycans and GAGs within the mitral valve leaflets, suggest that defects in valve maturation may be responsible for the myxomatous phenotype. It remains to be elucidated how perturbation of the balance of these cell populations within the valve may drive abnormal development as well as which cell population within the valve is responsible for the phenotype observed.

CONCLUSIONS

The results presented in this paper demonstrate that Bmp signaling at the AV junction through Alk3 is of critical importance to the development of the AV sulcus, annulus fibrosus, and AV valves. In embryonic $Wt1^{cre};Alk3^{fl/fl};R26^{mG}$ specimens, the AV sulcus and annulus fibrosus are hypoplastic and malformed. This phenotype is also observed in adult specimens indicating that Bmp signaling is required for formation of these structures and the observed abnormalities are not a consequence of developmental delay. In addition, the number of EPDCs that migrate into the parietal leaflets of the AV valves is significantly reduced in the $Wt1^{cre};Alk3^{fl/fl};R26^{mG}$ mouse. While the valves in $Wt1^{cre};Alk3^{fl/fl};R26^{mG}$ mice do not appear to be abnormal in embryonic stages, the observed valve pathology in the post-natal heart indicates that a normal contribution of EPDCs to the parietal leaflets is crucial for proper maturation. The reduced contribution of EPDCs to the left parietal leaflet and the development of the myxomatous valve phenotype generate interesting questions about the role of EPDCs in the etiology of myxomatous valve degeneration in human heart disease.

Acknowledgments

The authors would like to acknowledge the financial support by the following grants: NIH NCRR C06-RR018823, NIH-NCRR C06-RR015455, the “South Carolina COBRE for Developmentally Based Cardiovascular Diseases”, P30 GM103342-01 (A.W., T.T.), R01HL033756-30 (A.W., R.A.N.), American Heart Association Grant-in-Aid 13GRNT16220004 (A.W.), American Heart Association Predoctoral grant 12PRE11340000 (M.M.L.), Scientist Development Grant 11SDG527000 (R.A.N.), Leducq Foundation 07CVD04 (R.A.N.), NIH P20 GM103444-06 (R.A.N.), European Community’s Sixth Framework Program Grant LSHM-CT-2005-018630 (MJBvdH), Netherlands Heart Foundation Grant 1996M002 (MJBvdH), and The Foundation Leducq (Paris, France) Transatlantic Mitral Network of Excellence grant 07CVD04 (R.A.N.). This publication was supported by Project 1233 from the South Carolina Clinical & Translational Research (SCTR) Institute, with an academic home at the Medical University of South Carolina CTSA, NIH Grant Numbers UL1RR029882 and UL1TR000062. The contents are solely the responsibility of the authors and do not necessarily represent the official views of the NIH and AHA.

References

Aanhaanen W, Boukens B, Sizarov A, Wakker V, de Gier-de Vries C, van Ginneken A, Moorman A, Coronel R, Christoffels V. Defective Tbx2-dependent patterning of the atrioventricular canal myocardium causes accessory pathway formation in mice. The Journal of clinical investigation. 2011; 121:534–544. [PubMed: 21266775]

Barbara, PdS; Williams, J.; Goldstein, AM.; Doyle, AM.; Nielsen, C.; Winfield, S.; Faure, S.; Roberts, DJ. Bone morphogenetic protein signaling pathway plays multiple roles during gastrointestinal tract development. Developmental Dynamics. 2005; 234:312–322. [PubMed: 16110505]

Boukens B, Hoogendijk M, Verkerk A, Linnenbank A, van Dam P, Remme C-A, Fiolet J, Opthof T, Christoffels V, Coronel R. Early repolarization in mice causes overestimation of ventricular activation time by the QRS duration. Cardiovascular research. 2013; 97:182–191. [PubMed: 22997159]

Briggs L, Phelps A, Brown E, Kakarla J, Anderson R, van den Hoff M, Wessels A. Expression of the BMP receptor Alk3 in the second heart field is essential for development of the dorsal mesenchymal protrusion and atrioventricular septation. Circulation research. 2013; 112:1420–1432. [PubMed: 23584254]

Casanova, JsC; Travisano, S.; de la Pompa, JL. Epithelial-to-mesenchymal transition in epicardium is independent of Snail1. Genesis (New York, N Y : 2000). 2012; 51:32–40.

de Lange F, Moorman A, Anderson R, Männer J, Soufan A, de Gier-de Vries C, Schneider M, Webb S, van den Hoff M, Christoffels V. Lineage and morphogenetic analysis of the cardiac valves. Circulation research. 2004; 95:645–654. [PubMed: 15297379]

Dietz H, Cutting G, Pyeritz R, Maslen C, Sakai L, Corson G, Puffenberger E, Hamosh A, Nanthakumar E, Curristin S. Marfan syndrome caused by a recurrent de novo missense mutation in the fibrillin gene. Nature. 1991; 352:337–339. [PubMed: 1852208]

Gaussin V, Morley G, Cox L, Zwijsen A, Vance K, Emile L, Tian Y, Liu J, Hong C, Myers D, Conway S, Depre C, Mishina Y, Behringer R, Hanks M, Schneider M, Huylebroeck D, Fishman G, Burch J, Vatner S. Alk3/Bmpr1a receptor is required for development of the atrioventricular canal into valves and annulus fibrosus. Circulation research. 2005; 97:219–226. [PubMed: 16037571]

Gaussin V, Van de Putte T, Mishina Y, Hanks M, Zwijsen A, Huylebroeck D, Behringer R, Schneider M. Endocardial cushion and myocardial defects after cardiac myocyte-specific conditional deletion of the bone morphogenetic protein receptor ALK3. Proceedings of the National Academy of Sciences of the United States of America. 2002; 99:2878–2883. [PubMed: 11854453]

Gupta V, Barzilla J, Mendez J, Stephens E, Lee E, Collard C, Laucirica R, Weigel P, Grande-Allen K. Abundance and location of proteoglycans and hyaluronan within normal and myxomatous mitral valves. Cardiovascular pathology : the official journal of the Society for Cardiovascular Pathology. 2009; 18:191–197. [PubMed: 18621549]

Hayek E, Gring CN, Griffin BP. Mitral Valve Prolapse. The Lancet. 2005; 365:507–518.

Hill C, Sanchez N, Love J, Arrieta J, Hong C, Brown C, Austin A, Barnett J. BMP2 signals loss of epithelial character in epicardial cells but requires the Type III TGFβ receptor to promote invasion. Cellular signalling. 2012; 24:1012–1022. [PubMed: 22237159]

Jaffe A, Geltman E, Rodey G, Uitto J. Mitral valve prolapse: a consistent manifestation of type IV Ehlers-Danlos syndrome. The pathogenetic role of the abnormal production of type III collagen. Circulation. 1981; 64:121–125. [PubMed: 7237708]

Jensen B, Boukens B, Postma A, Gunst Q, van den Hoff M, Moorman A, Wang T, Christoffels V. Identifying the evolutionary building blocks of the cardiac conduction system. PloS one. 2012; 7

Jiao K, Kulessa H, Tompkins K, Zhou Y, Batts L, Baldwin H, Hogan B. An essential role of Bmp4 in the atrioventricular septation of the mouse heart. Genes & development. 2003; 17:2362–2367. [PubMed: 12975322]

Kolditz D, Wijffels M, Blom N, van der Laarse A, Hahurij N, Lie-Venema H, Markwald R, Poelmann R, Schalij M, Gittenberger-de Groot A. Epicardium-derived cells in development of annulus fibrosis and persistence of accessory pathways. Circulation. 2008; 117:1508–1517. [PubMed: 18332266]

Kruithof B, Krawitz S, Gaussin V. Atrioventricular valve development during late embryonic and postnatal stages involves condensation and extracellular matrix remodeling. Developmental biology. 2007; 302:208–217. [PubMed: 17054936]

Kruithof B, van Wijk B, Somi S, Kruithof-de Julio M, Perez Pomares J, Weesie F, Wessels A, Moorman A, van den Hoff M. BMP and FGF regulate the differentiation of multipotential pericardial mesoderm into the myocardial or epicardial lineage. Developmental biology. 2006; 295:507–522. [PubMed: 16753139]

Kubalak S, Miller-Hance W, O'Brien T, Dyson E, Chien K. Chamber specification of atrial myosin light chain-2 expression precedes septation during murine cardiogenesis. The Journal of biological chemistry. 1994; 269:16961–16970. [PubMed: 8207020]

Lepeschkin E, Surawicz B. The measurement of the Q-T interval of the electrocardiogram. Circulation. 1952; 6:378–388. [PubMed: 14954534]

Ma L, Lu M-F, Schwartz R, Martin J. Bmp2 is essential for cardiac cushion epithelial-mesenchymal transition and myocardial patterning. Development (Cambridge, England). 2005; 132:5601–5611.

Markwald RR, Fitzharris TP, Manasek FJ. Structural development of endocardial cushions. Am J Anat. 1977; 148:85–119. [PubMed: 842477]

Mishina Y, Hanks M, Miura S, Tallquist M, Behringer R. Generation of Bmpr/Alk3 conditional knockout mice. Genesis (New York, N Y : 2000). 2002; 32:69–72.

Mitchell G, Jeron A, Koren G. Measurement of heart rate and Q-T interval in the conscious mouse. The American journal of physiology. 1998; 274:51.

Ng CM, Cheng A, Myers LA, Martinez-Murillo F, Jie C, Bedja D, Gabrielson KL, Hausladen JM, Mecham RP, Judge DP, Dietz HC. TGF-beta-dependent pathogenesis of mitral valve prolapse in a mouse model of Marfan syndrome. J Clin Invest. 2004; 114:1586–1592. [PubMed: 15546004]

Rabkin E, Aikawa M, Stone J, Fukumoto Y, Libby P, Schoen F. Activated interstitial myofibroblasts express catabolic enzymes and mediate matrix remodeling in myxomatous heart valves. Circulation. 2001; 104:2525–2532. [PubMed: 11714645]

Rivera-Feliciano J, Tabin C. Bmp2 instructs cardiac progenitors to form the heart-valve-inducing field. Developmental biology. 2006; 295:580–588. [PubMed: 16730346]

Song L, Fassler R, Mishina Y, Jiao K, Baldwin H. Essential functions of Alk3 during AV cushion morphogenesis in mouse embryonic hearts. Developmental biology. 2007; 301:276–286. [PubMed: 16959237]

Tamura K, Fukuda Y, Ishizaki M, Masuda Y, Yamanaka N, Ferrans VJ. Abnormalities in elastic fibers and other connective-tissue components of floppy mitral valve. American heart journal. 1995; 129:1149–1158. [PubMed: 7754947]

Torihashi S, Hattori T, Hasegawa H, Kurahashi M, Ogaeri T, Fujimoto T. The expression and crucial roles of BMP signaling in development of smooth muscle progenitor cells in the mouse embryonic gut. Differentiation; research in biological diversity. 2009; 77:277–289.

van Wijk B, Moorman A, van den Hoff M. Role of bone morphogenetic proteins in cardiac differentiation. Cardiovascular research. 2007; 74:244–255. [PubMed: 17187766]

Viragh S, Challice C. The origin of the epicardium and the embryonic myocardial circulation in the mouse. The Anatomical record. 1981; 201:157–168. [PubMed: 7305017]

von Gise A, Pu W. Endocardial and epicardial epithelial to mesenchymal transitions in heart development and disease. Circulation research. 2012; 110:1628–1645. [PubMed: 22679138]

Wessels A, van den Hoff MJ, Adamo RF, Phelps AL, Lockhart MM, Sauls K, Briggs LE, Norris RA, van Wijk B, Perez-Pomares JM, Dettman RW, Burch JB. Epicardially derived fibroblasts preferentially contribute to the parietal leaflets of the atrioventricular valves in the murine heart. Developmental Biology. 2012; 366:111–124. [PubMed: 22546693]

Wilm B, Ipenberg A, Hastie ND, Burch JBE, Bader DM. The serosal mesothelium is a major source of smooth muscle cells of the gut vasculature. Development. 2005; 132:5317–5328. [PubMed: 16284122]

Yamada M, Revelli J, Eichele G, Barron M, Schwartz R. Expression of chick Tbx-2, Tbx-3, and Tbx-5 genes during early heart development: evidence for BMP2 induction of Tbx2. Developmental Biology. 2000; 228:95–105. [PubMed: 11087629]

Zhou B, von Gise A, Ma Q, Hu Y, Pu W. Genetic fate mapping demonstrates contribution of epicardium-derived cells to the annulus fibrosis of the mammalian heart. Developmental Biology. 2010; 338:251–261. [PubMed: 20025864]

Highlights

- Epicardial Alk3 expression is important for atrioventricular (AV) sulcus formation
- Epicardial Alk3 expression is important for formation of annulus fibrosus
- Deletion of epicardial Alk3 inhibits migration of EPDCs into AV valve leaflets
- Reduced numbers of EPDCs in valve leaflets lead to myxomatous valve phenotype
- EPDCs are critically important for normal AV valve maturation

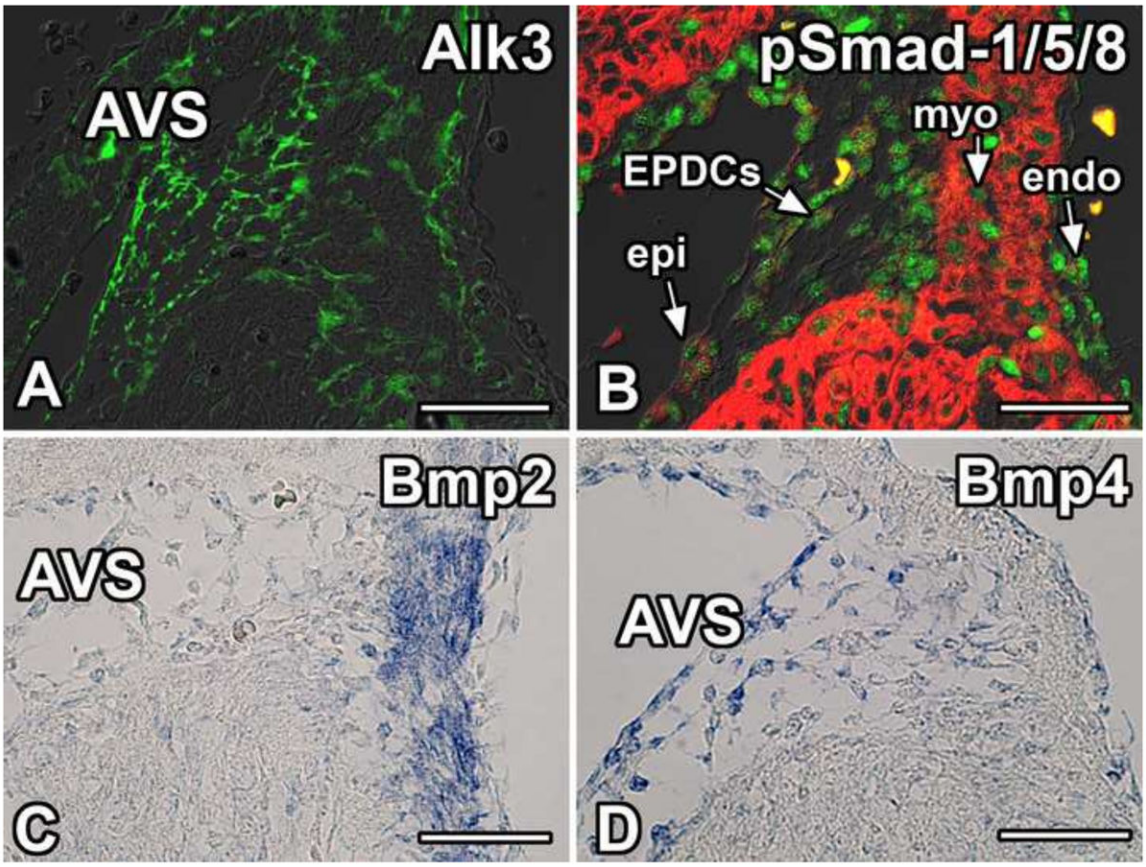

Figure 1. BMP signaling in the AV junction

Immunolabeling for Alk3 (green, A), pSmad-1/5/8 (green, B), and Myosin Heavy Chain (red, B) in the right AV junctional tissues of wildtype mice at ED13. Panel A shows that Alk3 is expressed throughout the AV sulcus and, to a lesser extent, the myocardium. Panel B shows that canonical Bmp signaling is active in the epicardium/EPDCs, the AV myocardium, and the endocardium. Panels C and D show *in situ* hybridization of wildtype mice at ED13.5 with probes recognizing Bmp2 (C) and Bmp4 (D) illustrating that Bmp2 is expressed in the AV junctional myocardium while Bmp4 is expressed in the AV sulcus and AV epicardium. (Scale bar = 50μm). AVS, AV sulcus; endo, endocardium; EPDCs, epicardially-derived cells; epi, epicardium; myo, myocardium.

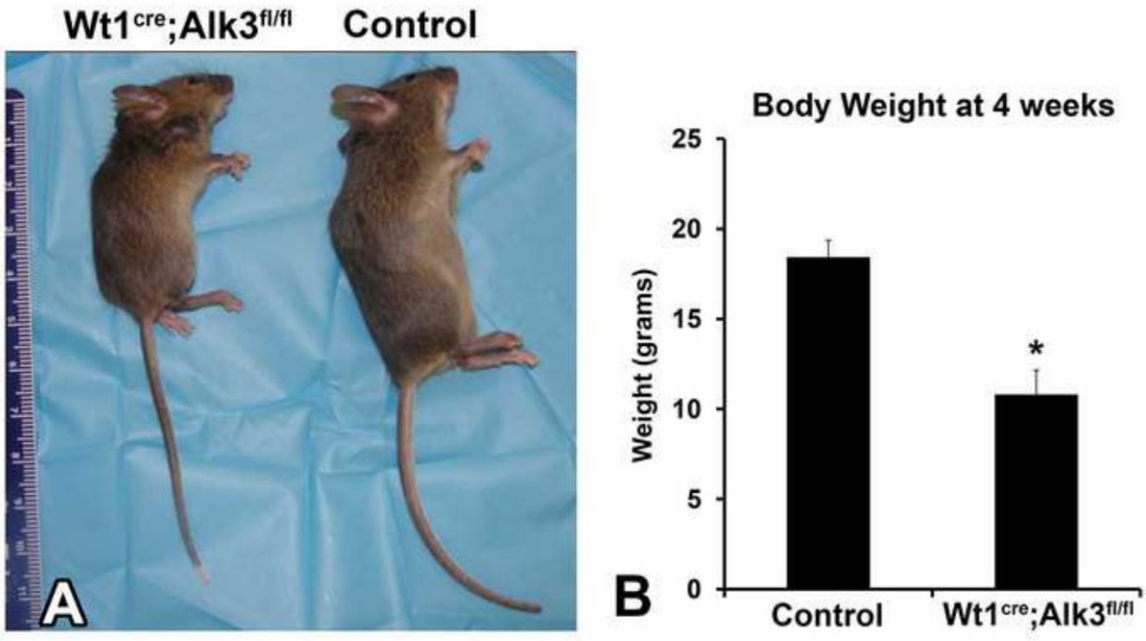

Figure 2. Wt1^{cre};Alk3$^{fl/fl}$ mice fail to thrive

A side-by-side comparison of four week old female specimens shows that the Wt1^{cre};Alk3$^{fl/fl}$ mouse is significantly smaller that the control littermate (A). Panel B shows the average body weight in grams of control and Wt1^{cre};Alk3$^{fl/fl}$ mice at four weeks of age. *$p<0.05$, $n=8$.

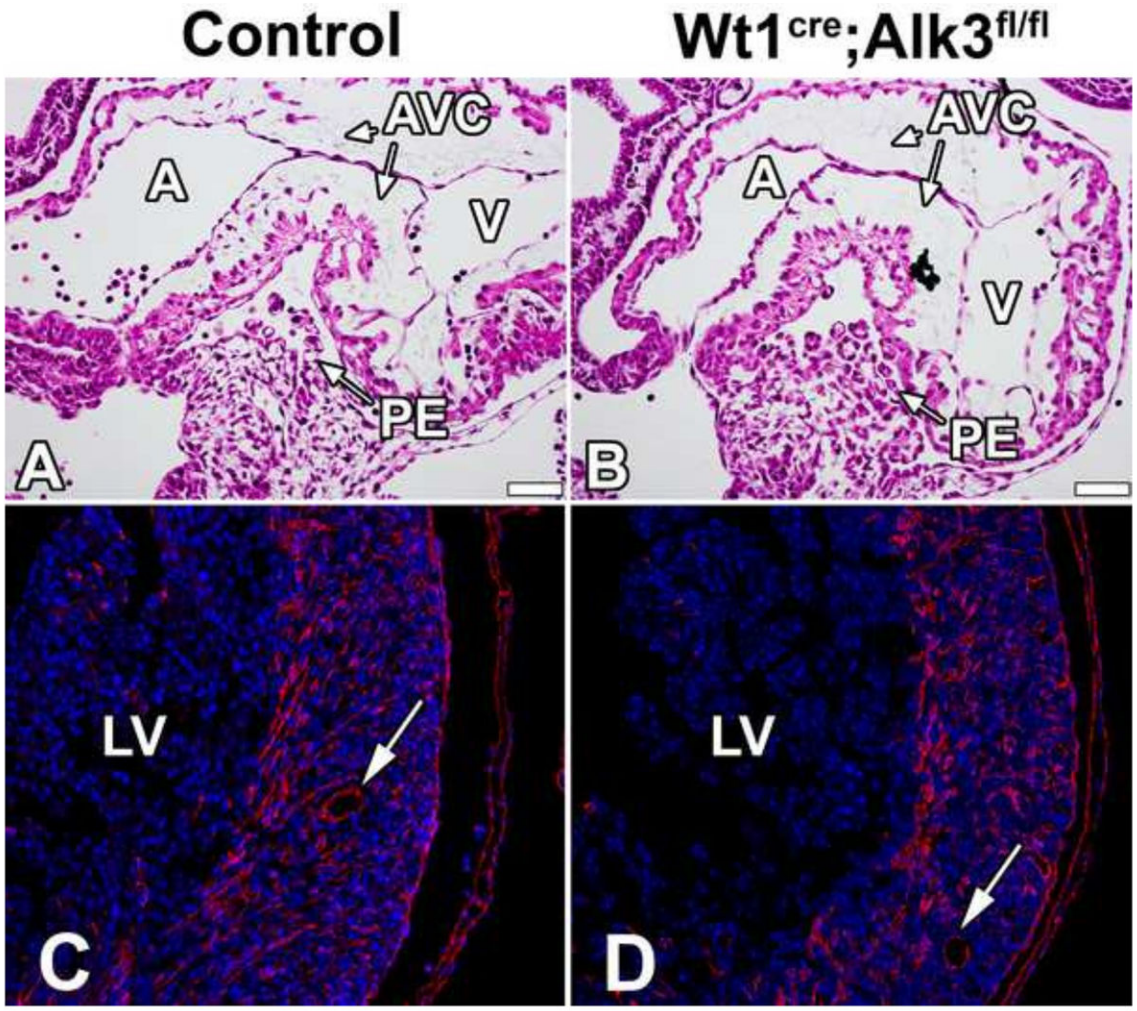

Figure 3. Proepicardium formation and EPDC contribution to the LV is unaffected in $Wt1^{cre};Alk3^{fl/fl};R26^{mG}$ hearts

H/E stained sections of ED9.5 control (A) and $Wt1^{cre};Alk3^{fl/fl}$ (B) specimens show normal formation of the proepicardium. ED17 control (C) and $Wt1^{cre};Alk3^{fl/fl};R26^{mG}$ (D) specimens immunolabeled for DAPI (blue) and eGFP (red) demonstrate that EPDC contribution to the LV is unaltered in the $Wt1^{cre};Alk3^{fl/fl};R26^{mG}$ hearts. Arrows indicate EPDC contribution to the coronary vasculature. (Scale bar = 50μm). A, atria; AVC, atrioventricular cushion; LV, left ventricle; PE, proepicardium; V, ventricle.

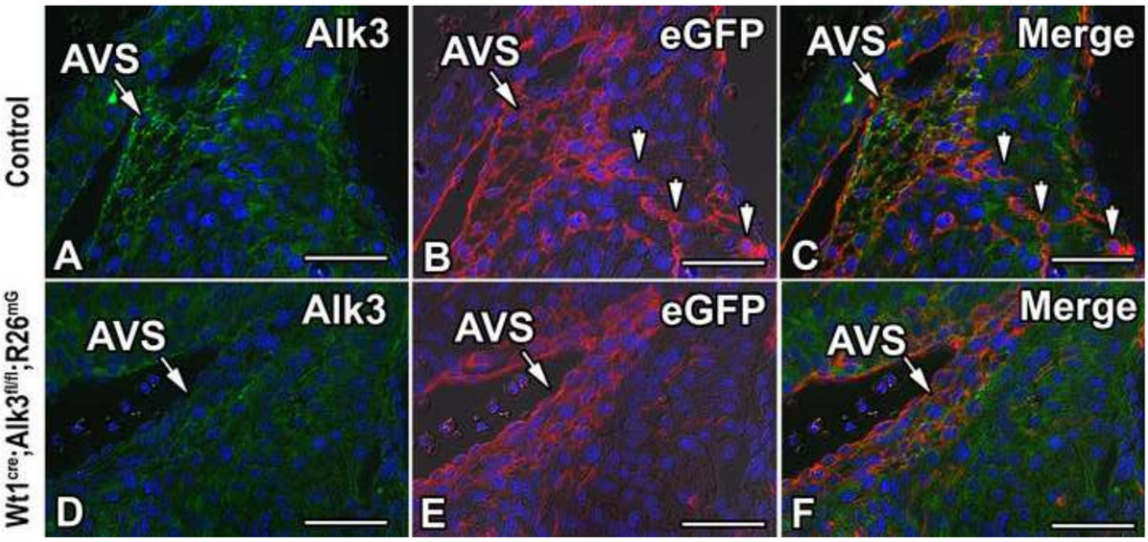

Figure 4. Loss of Alk3 expression in the AV sulcus of $Wt1^{cre}$;$Alk3^{fl/fl}$;$R26^{mG}$ mice

Immunolabeling for Alk3 (green, A, C, D, F), eGFP (red, B, C, E, F), and DAPI (blue, A- F) in the right AV junction of ED13 control (A-C) and $Wt1^{cre}$;$Alk3^{fl/fl}$;$R26^{mG}$ (D-F) specimens. In panel C, the channels depicted in A and B are merged, while in panel F the channels depicted in D and E are merged. Panels A-C show that Alk3 is expressed in the eGFP labeled EPDCs of the AV sulcus. Panels D-F show that in $Wt1^{cre}$;$Alk3^{fl/fl}$;$R26^{mG}$ mice Alk3 is efficiently deleted from the EPDCs in the AV sulcus. Arrowheads in B, C indicate eGFP labeled EPDCs within the AV canal myocardium of the control specimen. (Scale bar = 50μm). AVS, AV sulcus.

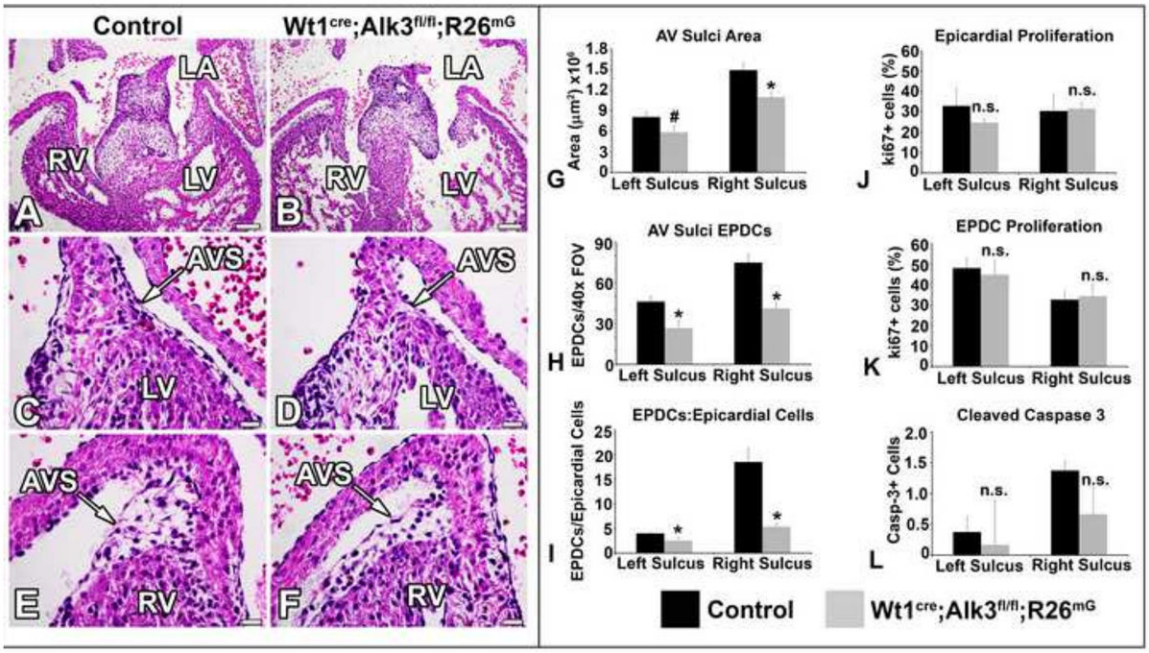

Figure 5. Loss of Alk3 in EPDCs results in hypoplasia of the AV sulcus

Panels A-F show H/E stained sections of ED13 control (A,C,E) and Wt1^{cre};Alk3$^{fl/fl}$;R26^{mG} (B,D,F) hearts. The staining reveals hypoplastic AV sulci in the Wt1^{cre};Alk3$^{fl/fl}$;R26^{mG} heart at the left (D) and right (F) AV junctions. (G) Quantification of left and right AV sulcus areas shows a significant reduction in AV sulci size. (H) Hypoplasia of the left and right AV sulcus is due to a significantly decreased number of EPDCs within the tissue. (I) The ratio of AV sulcus EPDCs to AV epicardial cells is significantly reduced in Wt1^{cre};Alk3$^{fl/fl}$;R26^{mG} hearts. Despite a significant reduction in the number of AV sulcus EPDCs, the percentage of proliferating (ki67+) AV sulcus EPDCs (J) and overlying AV epicardial cells (K) is not significantly different between control and Wt1^{cre};Alk3$^{fl/fl}$;R26^{mG} specimens. (L) Apoptosis of AV EPDCs, marked by Cleaved Caspase 3, is not significantly different in Wt1^{cre};Alk3$^{fl/fl}$;R26^{mG} hearts. (Scale bars in A and B=100μm, scale bars in C-F=20μm); n≥3; *=p<0.05, #=p<0.1, n.s.= not statistically significant. AVS, AV sulcus; LA, left atria; LV, left ventricle; RV, right ventricle.

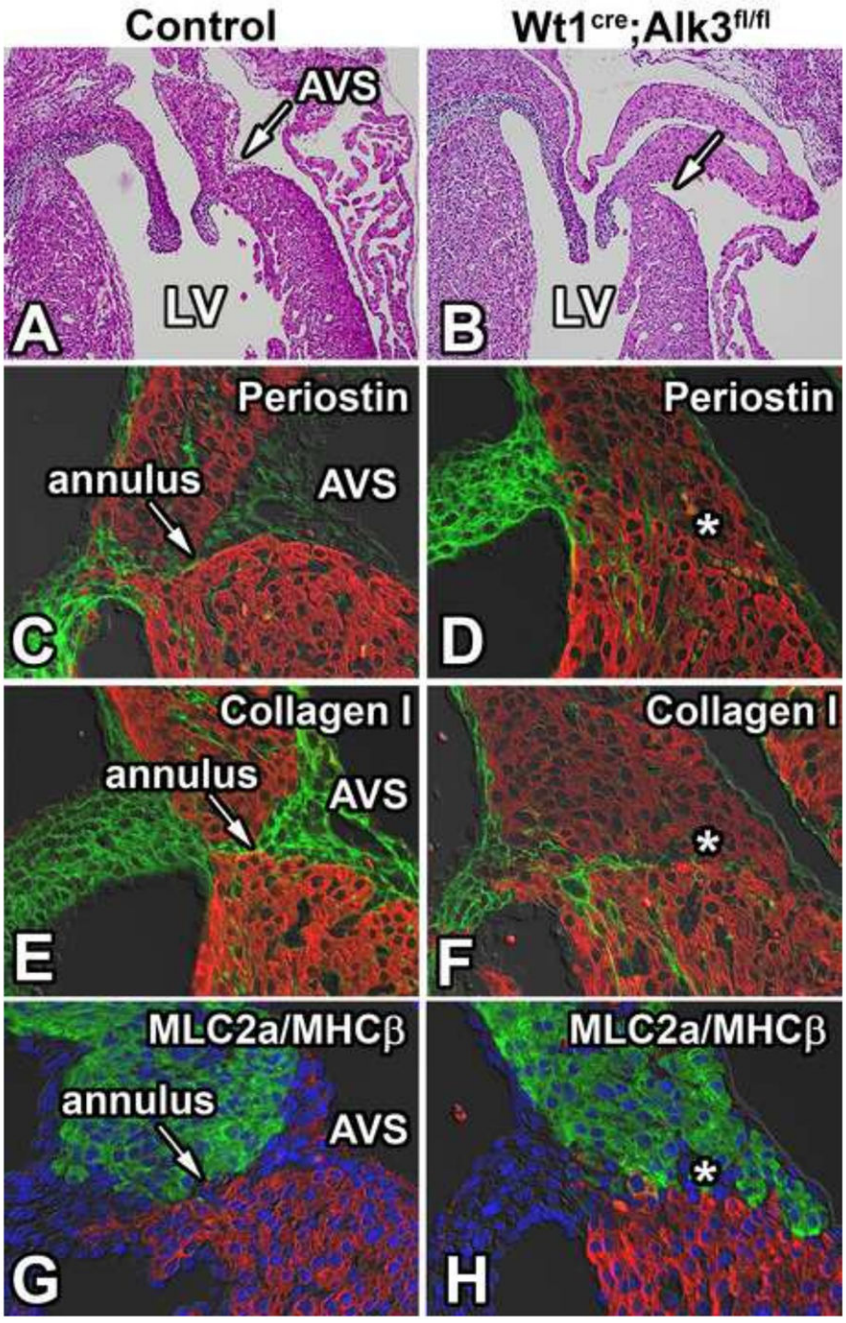

Figure 6. Loss of Alk3 in EPDCs results in malformation of the annulus fibrosus

Panels A and B show the left AV junction of H/E stained sections of ED17 control and $Wt1^{cre}$;$Alk3^{fl/fl}$;$R26^{mG}$ hearts. The AV sulcus is absent in the left AV junction of the $Wt1^{cre}$;$Alk3^{fl/fl}$;$R26^{mG}$ heart (B). Immunolabeling for MF20 (red, C-F), periostin (green; C,D) and collagen I (green; E,F) in these specimens shows that the annulus fibrosus, present in the control heart (arrow in C,E,G), is absent in the $Wt1^{cre}$;$Alk3^{fl/fl}$;$R26^{mG}$ heart (asterisk in panels D, E, and H). Immunolabeling for MLC2a (green; G,H), MHCβ (red; G,H), and DAPI (blue; G,H) marks where the atrial (MLC2a) and ventricular myocardium (MHCβ) meet in the AV junction. AVS, AV sulcus; LA, left atria; LV, left ventricle.

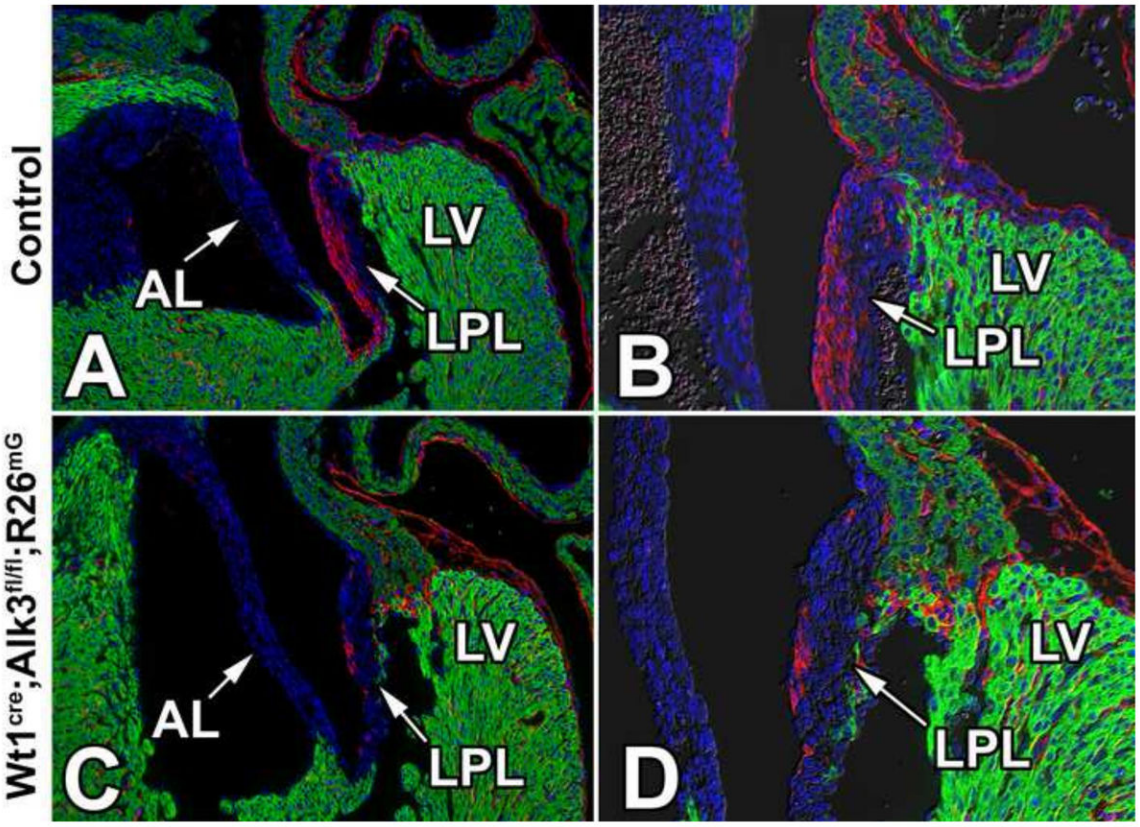

Figure 7. EPDCs fail to populate the parietal leaflets in $Wt1^{cre};Alk3^{fl/fl};R26^{mG}$ hearts

Immunolabeling for eGFP (red), MF20 (green), and nuclei/DAPI (blue) in ED17 control (A,B) and $Wt1^{cre};Alk3^{fl/fl};R26^{mG}$ (C,D) specimens. Panels C and D show a sharp reduction of eGFP-labeled EPDCs in the left parietal leaflet (LPL) of the $Wt1^{cre};Alk3^{fl/fl};R26^{mG}$ mouse. AL, aortic leaflet; LPL, left parietal leaflet; LV, left ventricle.

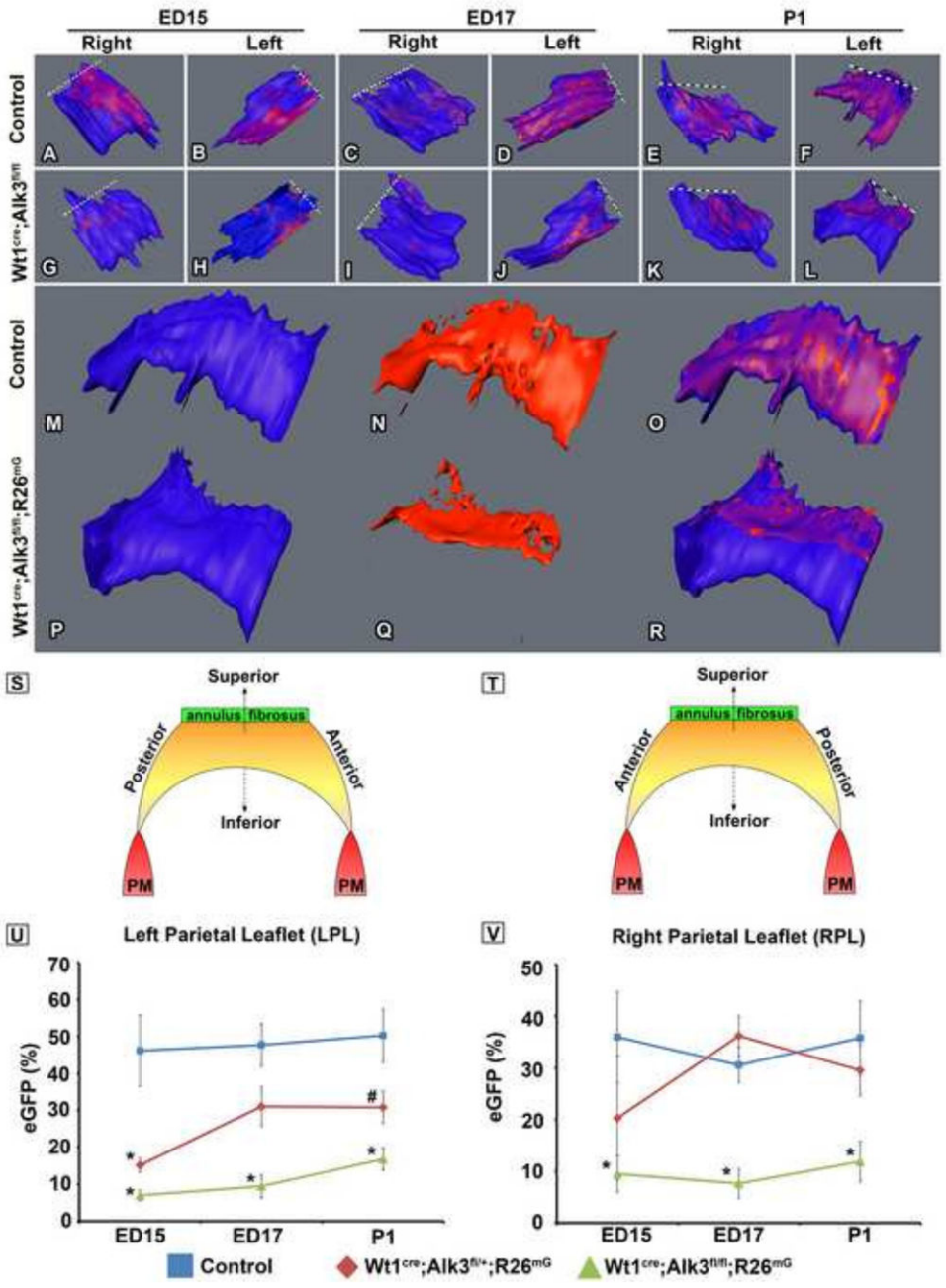

Figure 8. Spatiotemporal Assessment of the distribution of eGFP labeled EPDCs within the parietal leaflets

Panels A-R show 3D reconstructions of the right parietal leaflets (RPL) and the left parietal leaflets (LPL) from control and $Wt1^{cre};Alk3^{fl/fl};R26^{mG}$ specimens staged ED15, ED17, and postnatal day 1 (P1). The dashed lines in panels A-L indicate the location of the distal end of the leaflet where it connects to the annulus fibrosis. Panels M-R depict neonatal LPLs (blue; M,P) and the spatiotemporal contribution of EPDCs (red; N,Q) in control (M-O) and $Wt1^{cre};Alk3^{fl/fl};R26^{mG}$ hearts (P-R). Panels S and T are schematically depicting the structure and orientation of the LPL and the RPL as well as the associated anatomic descriptors. In panels U and V the EPDC contribution to the parietal leaflets in control,

$Wt1^{cre}$;$Alk3^{fl/+}$;$R26^{mG}$, and $Wt1^{cre}$;$Alk3^{fl/fl}$;$R26^{mG}$ specimens at each stage is quatified. The volume of eGFP+ cells was divided by the total volume of the valve. At ED15, ED17, and P1 the percentage of eGFP positive cells within the LPL (U) and RPL (V) is significantly decreased in $Wt1^{cre}$;$Alk3^{fl/fl}$;$R26^{mG}$ hearts. n≥3 for ED15 and P1, n≥2 for ED17; *=$p<0.05$, AL, aortic leaflet; LPL, left parietal leaflet; LV, left ventricle.

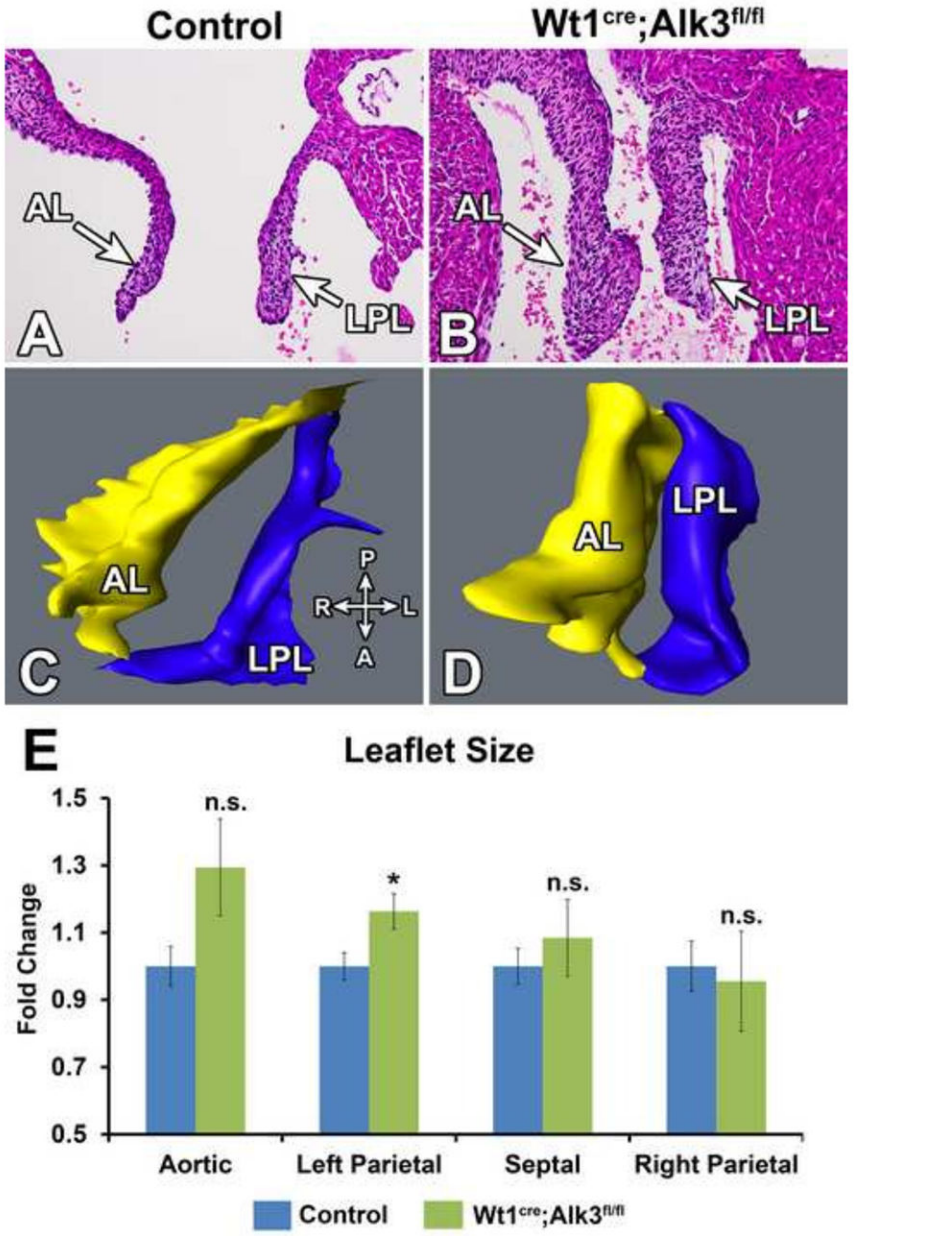

Figure 9. Increased leaflet size in neonatal mitral valves of Wt1^{cre};Alk3$^{fl/fl}$;R26^{mG} hearts

Panels A and B show Hematoxylin and Eosin stained neonatal control (A) and Wt1^{cre};Alk3$^{fl/fl}$;R26^{mG} (B) hearts. Panel B demonstrates that the AL and LPL of the mitral valve is enlarged in the Wt1^{cre};Alk3$^{fl/fl}$;R26^{mG} heart. Panels C and D show 3D reconstructions of the mitral valves shown in panels A and B. The compass in the lower right of panel C provides the anatomic orientation of the 3D rendering with the posterior (P) and anterior (A) on the vertical axis and right (R) and left (L) on the horizontal axis. Panel E shows the quantification of the valve volume as obtained by 3D AMIRA reconstruction. Valve volume is expressed as fold change over control. The volumes of the LPL in Wt1^{cre};Alk3$^{fl/fl}$;R26^{mG} neonatal specimens was significantly larger than that of the controls while the AL, SL and RPL were not significantly different. n≥5; *p=<0.05, A, anterior; AL,

aortic leaflet; D, distal: L, left; LPL, left parietal leaflet; P, posterior; R, right; RPL, right parietal leaflet.

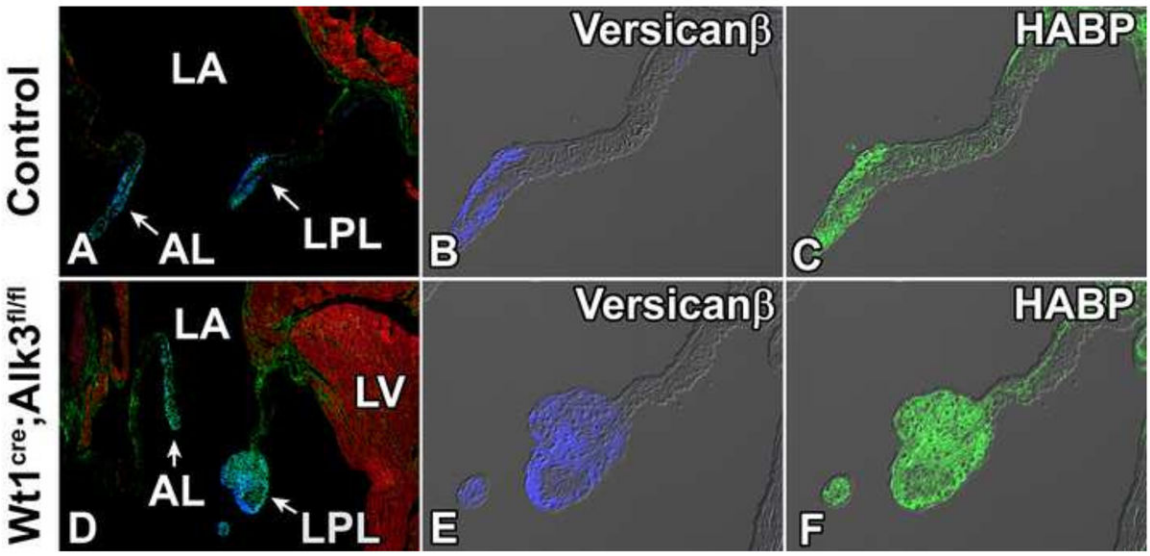

Figure 10. Wt1^{cre};Alk3$^{fl/fl}$;R26^{mG} mice have myxomatous mitral valves

Sections were immunolabeled for MF20 (red, A and D) to mark the myocardium. Immunostaining for Versican-β (blue, B and E), and HABP (green, C and F) shows expanded expression of Versican-β and Hyaluronan in the LPL of the Wt1^{cre};Alk3$^{fl/fl}$;R26^{mG} heart. AL, aortic leaflet; HABP, hyaluronan binding protein; LA, left atrium; LPL, left parietal leaflet; LV, left ventricle.

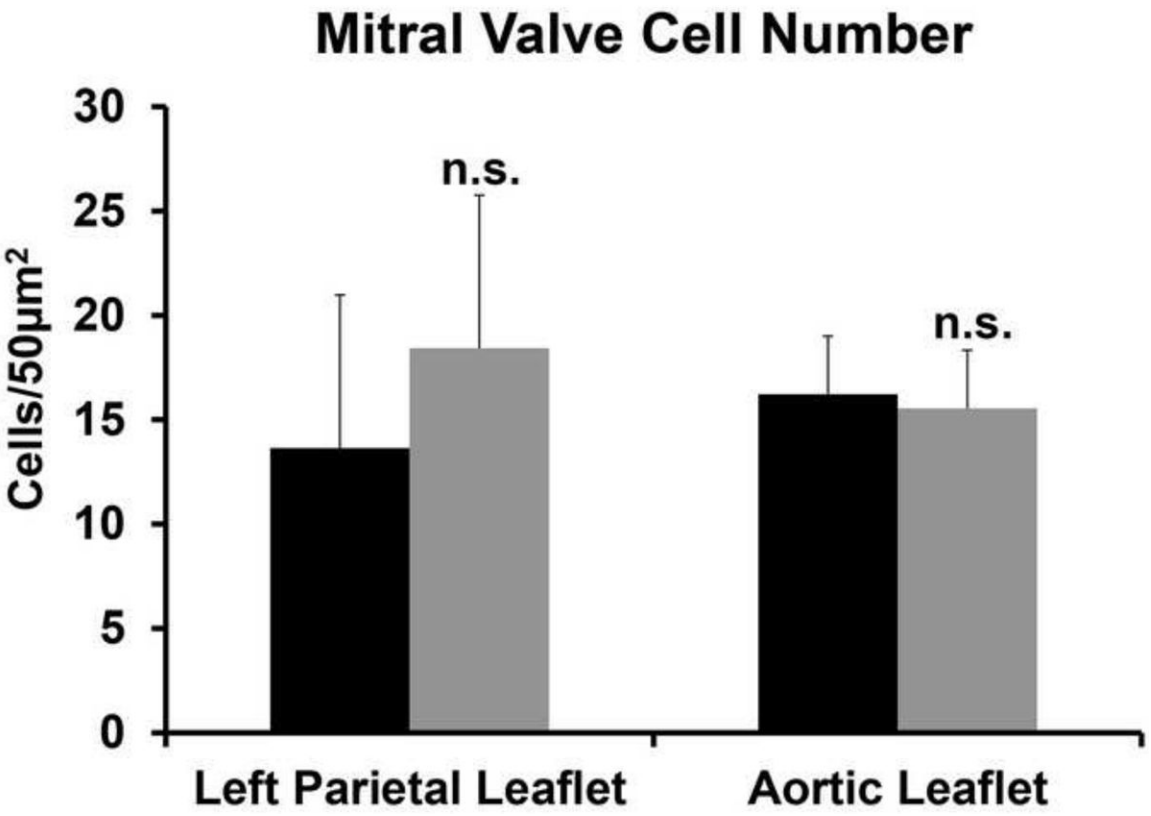

Figure 11. Cell number does not differ in control and Wt1^{cre};Alk3$^{fl/fl}$ mitral valve leaflets

The number of cells per 50μm^2 was evaluated in the LPL and AL in 1 month old control and Wt1^{cre};Alk3$^{fl/fl}$ mice. The number of cells was not significantly different in the LPL (p=0.51) or in the (p=0.87). (LPL, n=3; AL, n=4). n.s.; not significant

Table 1

Electrocardiogram

	Sample Size	PR Interval	QRS (lead III)	RR
Control	5	35.5± 1.8	8.4± 1.0	135.8± 16.9
$Wt1^{cre}$ $Alk3^{fl/fl}$;$R26^{mG}$	6	38.6± 3.9	7.3± 1.0	138.2± 23.8

Table 2

Proliferation in the Neonatal Left Parietal Leaflet

		% of total cells			% Proliferation	
	Total cell #	**EPDCs**	**non-EPDCs**	**All Cell Types**	**EPDCs**	**non-EPDCs**
Control	2052± 214	87.56± 1.15	12.44± 1.15	21.82± 1.47	23.46± 1.72	14.37± 4.33
$Wt1^{cre};Alk3^{fl/fl};R26^{mG}$	2299± 103	21± 2.46	79± 2.46	24.04± 5.01	30.84± 0.92*	22.20± 6.15

*$p<0.05$